journal

J. Am. Ceram. Soc., 91 [11] 3652–3658 (2008)
DOI: 10.1111/j.1551-2916.2008.02639.x

Formation of Oxide Scales on Zirconium Diboride–Silicon Carbide Composites During Oxidation: Relation of Subscale Recession to Liquid Oxide Flow

Sigrun N. Karlsdottir[†,‡] and John W. Halloran

Department of Materials Science and Engineering, University of Michigan, Ann Arbor, Michigan 48104

The formation of oxide scales on zirconium diboride (ZrB_2)–silicon carbide (SiC) composites oxidized at high temperatures (>1500°C) is studied. Subscale recession found in oxidized ZrB_2 composites is proposed to form due to flow of boron oxide (boria) (B_2O_3)-rich borosilicate liquid through convection cells that form upon oxidation of the composite at high temperatures. The flow of the B_2O_3-rich liquid to the surface, with the subsequent loss of B_2O_3 to evaporation, explains the formation of a glassy silica-rich layer on the surface commonly reported in the literature. Also the outward flow of the liquid creates a localized inward path for oxygen due to lower viscosity that allows faster oxidation under the convection cells which creates the subscale recession. Optical and electron micrographs of a ZrB_2–15%SiC composite oxidized at 1550°C are presented as evidence of flowing liquids. Micrographs of oxide scale deformations are also presented, which are proposed to be related to the formation of oxide scale features called convection cells. The subscale recession and oxide scale deformations of ZrB_2–15%SiC composites oxidized for 3 and 4 h at 1550°C were studied with microstructure and chemical composition analysis.

I. Introduction

The zirconium diboride (ZrB_2)–silicon carbide (SiC) and HfB_2–SiC composites oxidize to form a complex multilayer oxide scale at temperatures between 1400° and 1700°C.[1–3] Often the oxide scale features a silica (SiO_2)-rich outer layer, which lies over a subscale of crystalline zirconia (ZrO_2), often with a columnar microstructure with SiO_2 between the ZrO_2 grains. Depletion of SiC from the virgin material under the ZrO_2 scale has also been observed and reported.[4,5] While frequently observed, the mechanisms that form this complex scale are not understood in detail.[6,7] The interpretation of this complex oxide scale presents several puzzles. ZrO_2 appears often as a columnar subscale and as a noncolumnar phase in the SiO_2 layer. Depletion of SiC underneath the ZrO_2 scale suggests formation of SiO_2 liquid or SiO vapor *under* the ZrO_2, but most of the SiO_2 is found *over* the ZrO_2. The SiO_2 liquid can dissolve with boron oxide (boria) (B_2O_3) liquid (formed upon oxidation of ZrB_2) forming a borosilicate surface layer (B_2O_3–SiO_2). B_2O_3 is, however, largely absent, due to evaporation at higher temperatures. B_2O_3 has a vapor pressure of 233 Pa at 1500°C[8] while SiO_2 has a vapor pressure of 3×10^{-4} Pa.[5] How can these complex oxide scale features be interpreted?

Recently, Karlsdottir *et al.*[9] proposed that liquid flow of B_2O_3–SiO_2–ZrO_2 (BSZ) liquids plays an important role in the formation of these scales, based on distinctive microstructural features observed on the external oxide surface and in cross section.

These features are called convection cells. Figure 1 shows an example of these convection cells. The image shows a backscattering electron (BSE) image of a surface of a ZrB_2–15 vol% SiC specimen oxidized at 1600°C for 30 min. The surface of the oxidized specimen is covered with convection cells forming a pattern. The convection cells have ZrO_2 islands (white area) located in larger SiO_2-rich "lagoons"(gray area) with B_2O_3-rich patterns (dark contrast) surrounding the islands. The area around the convection cells consists of a SiO_2-rich glass (gray region) with small micrometer-sized ZrO_2 dispersoids (white dots). The B_2O_3 flower-like patterns are visible in BSE images, but in stronger contrast when imaged by cathodoluminescence (CL). The ZrO_2 islands have been proposed previously[9] to have formed by precipitation during the evaporation of B_2O_3 from a BSZ liquid that rises through an outer SiO_2-rich borosilicate layer and flows laterally by viscous fingering forming the B_2O_3-rich regions around the ZrO_2 islands.[9,10] The driving force is proposed to be the large volume increase upon oxidation of the bulk material due to the formation of solid ZrO_2(s) and BSZ liquid.[9] Figure 2 is a schematic of these convection cells and their formation.

These convection cell features had not been discussed by others before, but close examination of cross-sectional micrographs in the literature suggest that the features might have been observed, but have not be interpreted. In this paper the interpretation of oxide scale features of diboride–SiC composites will be discussed. Optical and electron micrographs will be presented as evidence of flowing liquids. Oxide scale deformation related to the formation of convection cell will also be presented and discussed. Finally, subscale recession found in oxide scales formed during oxidation of boride–SiC-based material are discussed in connection to convection cell features.

II. Experimental Procedure: Materials and Methods

ZrB_2–15 vol% SiC composite materials were fabricated at Institute of Science and Technology for Ceramics, National Research Council (CNR-ISTEC) in Faenza, Italy, using methods presented elsewhere.[11] Before testing, ca. 200 μm was removed from surface by diamond grinding (Omni Brade, TBW Industries, Furlong, PA). This was to remove any heat-affected zone that could have formed during wire electrical discharge machining (w-EDM) (Ann Arbor Machine Model 1S15, Ann Arbor, MI), which was used to cut the bulk material into thin sheets. The thin sheets of the ZrB_2–15 vol% SiC material were then cut with a diamond saw (IsoMet® 1000 diamond precision saw, Buehler, Lake Bluff, IL) into small rectangular coupons with total surface area on average of ca. 1 cm^2. They were oxidized at high temperatures in ambient air at temperatures between 1550° and 1600°C for different times ranging from ½ to 4 h. The tests were performed either in a high-temperature box furnace (SentroTech Corporation, Berea, OH) or in a tube-furnace (Lindberg, Watertown, WI). The heating rate used was 13°C/min with free cooling or with 13°C/min cooling rate. In the

H.-J. Kleebe—contributing editor

Manuscript No. 24490. Received March 31, 2008; approved July 10, 2008.
[†]Author to whom correspondence should be addressed. e-mail: nanna@umich.edu
[‡]Present address: Department of Materials, Biotechnology and Energy, Innovation Center Iceland, IS-112 Reykjavik, Iceland.

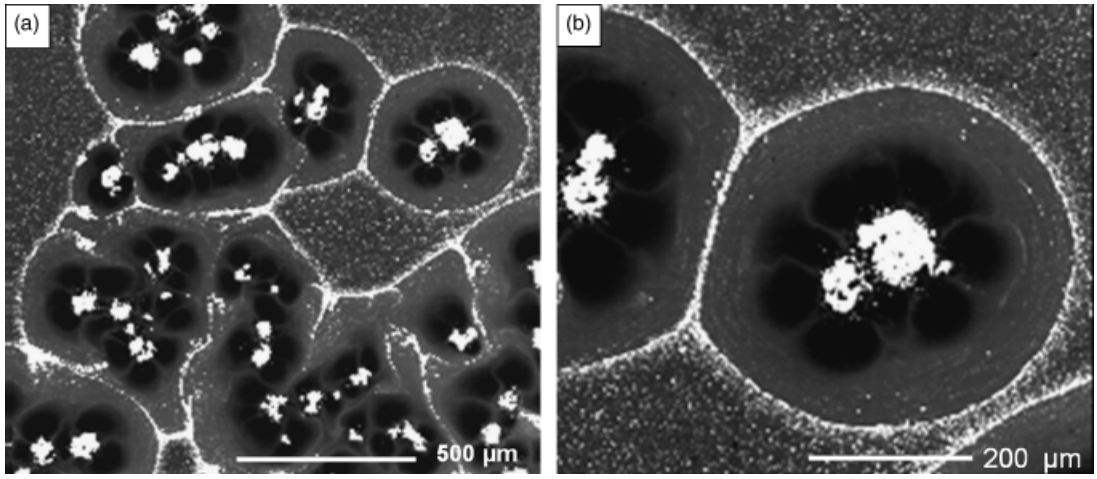

Fig. 1. Backscattered electron images of the surface of a ZrB_2–15 vol% SiC composite oxidized at 1600°C for 30 min. (a) Surface covered with convection cells that have ZrO_2 islands (white) located in larger SiO_2, lagoons (gray) with B_2O_3-rich patterns (black) surrounding the islands. (b) Higher magnification of a convection cell.

furnace the specimens were supported by the same material (ZrB_2–SiC) that was placed on an Al_2O_3 support in an Al_2O_3 crucible.

Chemical composition and microstructural analysis were done on the surfaces and cross sections of the oxidized specimens using bright field optical microscopy of the as-oxidized surface, scanning electron microscopy, BSE microscopy, and electron microprobe analyzer (EMPA). A Cameca SX100 was used for EMPA, using well-characterized mineral standards for quantitative analysis of boron (B), oxygen (O), zirconium (Zr), and silicon (Si), and for imaging in the BSE and CL modes. The EMPA standards and technique that were used are described in more detail elsewhere.[9] The cross sections of the oxidized specimens were prepared for microstructural analysis by nonaqueous polishing procedures down to 1 μm finish. Specimens were coated with carbon before microstructural and elemental analysis.

III. Interpretation of Oxide Scale

Examination of the surface of the oxidized samples provides clear evidence of liquid flow. Figure 3(a) is an optical micrograph of the surface after oxidation for 4 h at 1550°C. Optical metallograph image in reflected light shows what appears to be "islands" of ZrO_2 in a film of borosilicate glass. These islands are assemblies of ZrO_2 grains emerging from the once-liquid glassy surface. The darker regions of the glass are rich in SiO_2, and are dark because of the relative transparency scatters little of the incident light. Very small dispersed ZrO_2 particles barely visible are on the surface of the SiO_2. The cloudy features are subsurface B_2O_3-rich borosilicate. These borosilicate regions are turbid because of liquid–liquid phase separation in the glass during cooling. The appearance of the turbid and clear regions of the glass is suggestive of liquids flowing from the neighborhood of the ZrO_2 island. Figure 3(b) is a BSE image of the same field of view as Fig. 3(a). In BSE imaging, the ZrO_2 islands appear in bright contrast. The SiO_2-rich glassy regions appear in light gray contrast, and the B_2O_3-rich regions in darker contrast. The small dispersed ZrO_2 particles on the SiO_2 are highly visible. The arrangement of these small ZrO_2 dispersoids is hard to understand without presuming that they were arranged by flowing liquids. We present these images as evidence in support of the hypothesis of convective flow, as illustrated in the schematic of Fig. 2.

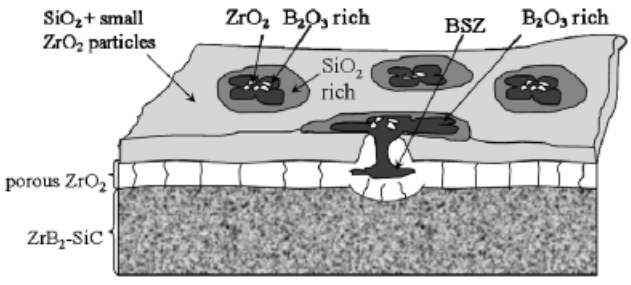

Fig. 2. Schematic of the convection cell features seen on surfaces and cross sections of ZrB_2–SiC composites oxidized at temperatures between 1500° and 1600°C. The schematic shows convection cells spread on the surface with their ZrO_2 islands (white) located in larger SiO_2, lagoons (light gray) with B_2O_3-rich patterns (dark gray) surrounding the islands.

Now let us direct our attention to cross section of the oxide scales. Figures 4(a)–(c) show BSE images of a cross section of a ZrB_2–15 vol% SiC specimen oxidized at 1550°C for 3 h in a tube-furnace in ambient air, with a heating rate of 13°C/min and free cooling. The images show significant deformations of the oxide scale. The SiO_2 outer scale appears in the BSE image in darker contrast, while the ZrO_2 subscale is in brighter contrast. The contrast between ZrO_2 and ZrB_2 is slight in this image. The higher magnifications, Figs. 4(b) and (c), show that the ZrO_2 scale is deformed; it appears to be lifted up, like a blister. Inside the "blister" is a glassy phase shown by EMPA maps and analysis to be rich in B_2O_3, SiO_2, and with some ZrO_2.

Figures 5(a)–(e) show a BSE image of one of the deformations shown in Fig. 4(a) and the corresponding EMPA maps of this area, showing the distribution of B, Si, O, and Zr. The distinction between the ZrO_2 in the primary scale and the ZrB_2 substrate can be made by comparing the zirconium image Fig. 5(c) with the boron image Fig. 5(e) and the oxygen image Fig. 5(b). Clearly the ZrB_2 substrate and the ZrO_2 primary scale are being separated by a liquid rich in O, Si, and B, with significant distortion of the ZrO_2 primary scale. Figure 6 shows the corresponding line analysis from these elemental maps, indicating that the glass inside the "blister" is rich in B_2O_3, and SiO_2, and has some ZrO_2. Based on a calculated ternary phase diagram of a ZrO_2–SiO_2–B_2O_3 system, an isothermal section at 1500°C, published previously by Karlsdottir *et al.*,[10] it is presumed that this material is the glass formed by cooling of a BSZ liquid in equilibrium with $ZrO_2(s)$ at this temperature (1550°C).

The driving force for these deformations is likely the very large volume increase upon oxidation of the bulk material due to the formation of condensed oxides, solid $ZrO_2(s)$ and BSZ liquid, where the oxide products occupy a volume 3.2 times as great as the ZrB_2–SiC substrate.[9] From the microstructural and chemical compositional analysis of the blisters (deformations) we propose that the BSZ liquid forms at the reaction interface, i.e. between a "primary" oxide scale (a thin outer SiO_2-rich borosilicate layer and an underlying porous $ZrO_2(s)$) and the unreacted bulk material. Here it is hypothesized that the blisters

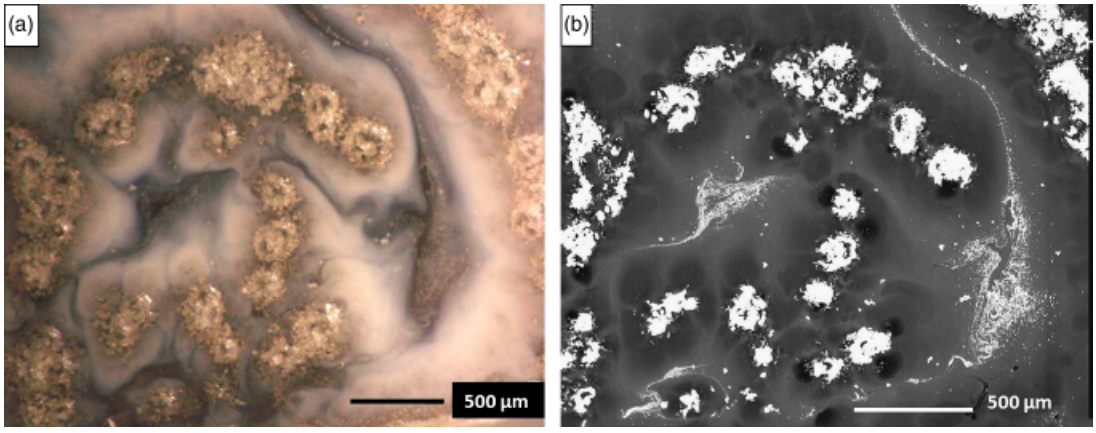

Fig. 3. Surface of an oxide scale on ZrB_2–15 vol% SiC composite after oxidation for 4 h at 1550°C. (a) Optical image in reflected light, showing "islands" of ZrO_2 in a film of borosilicate glass. The darker regions of the glass are rich in SiO_2, which are dark because of transparency, with small dispersed ZrO_2 particles barely visible. The cloudy regions are B_2O_3-rich borosilicate, turbid because of liquid–liquid phase separation in the glass during cooling, (b) backscattered electron image of the same region, where ZrO_2 islands appear in bright contrast, SiO_2-rich glassy regions in light gray contrast, and B_2O_3-rich regions in dark gray contrast. The small dispersed ZrO_2 particles on the SiO_2 appear in bright contrast.

form because of the large volume increase, induced by the formation of the oxides during oxidation. The large volume increase of the formed oxides induces pressure and stresses when the oxide scale grows leading to a rupture in the "primary" oxide scale. Our hypothesis is that the BSZ liquid at the reaction interface is then squeezed up to the surface where it starts flowing, forming the convection cells and their features.

Figure 4(d) shows a secondary electron image of a polished cross section of a convection cell on an oxidized ZrB_2–SiC sample. The sample was oxidized for 4 h at 1550°C in a tube-furnace in ambient air, with a heating rate of 13°C/min and free cooling. The image shows the SiO_2-rich external scale, in dark gray contrast, covering a ZrO_2 subscale (primary ZrO_2) in light gray contrast, over the unoxidized ZrB_2–SiC substrate. The ZrO_2 "island" impinging on the surface (formed by precipitation of ZrO_2) is seen in cross section to be a vertical feature containing region of glass in the middle. The glass contains B_2O_3, SiO_2, and some ZrO_2, it is also richer in boron (B) than the glass outside of

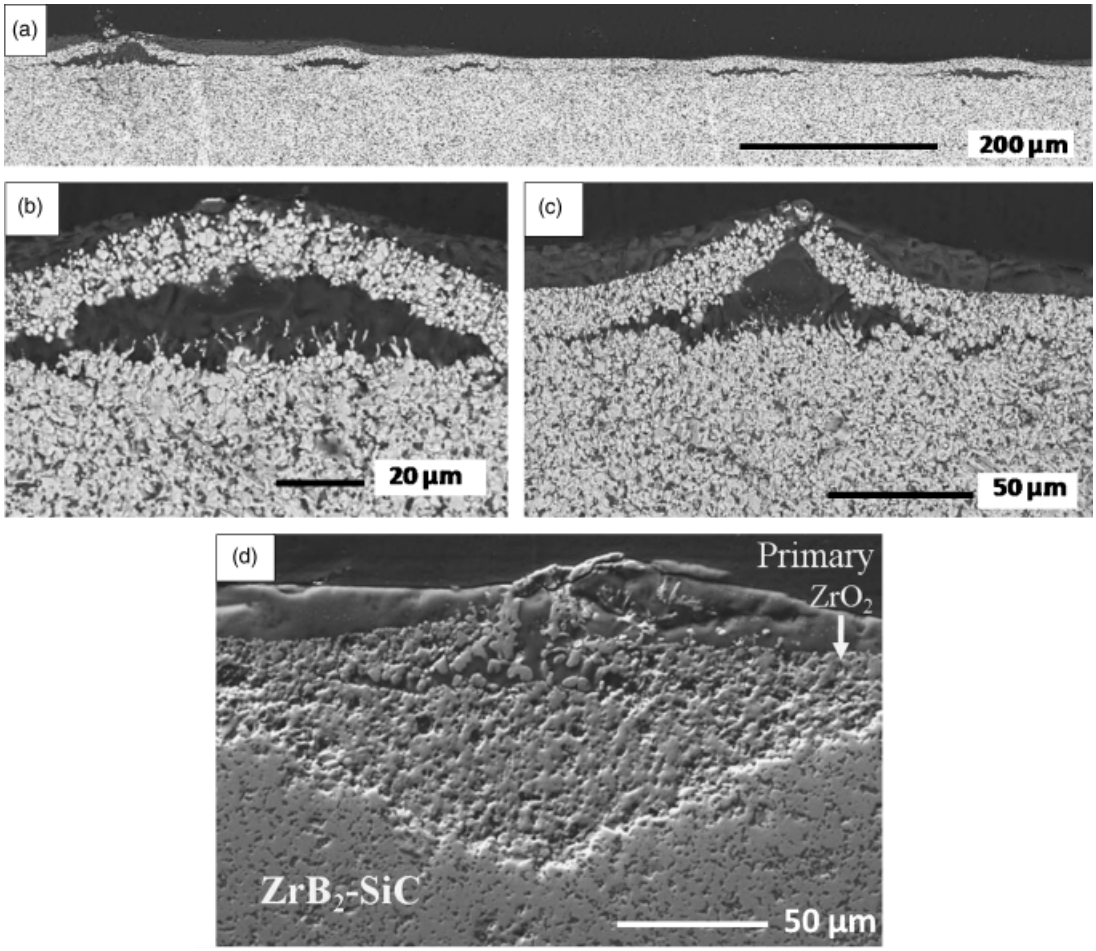

Fig. 4. (a)–(c) Backscattered electron images of cross sections of ZrB_2–15 vol% SiC composite oxidized for 3 h, showing the built up of the BSZ liquid between the "primary" oxide scale (SiO_2-rich top layer and an under laying ZrO_2) and the bulk material (ZrB_2–SiC). (d) Scanning electron microscopic image of a cross section of a convection cell on ZrB_2–SiC oxidized at 1550°C for 4 h, showing the inner structure of a convection cell.

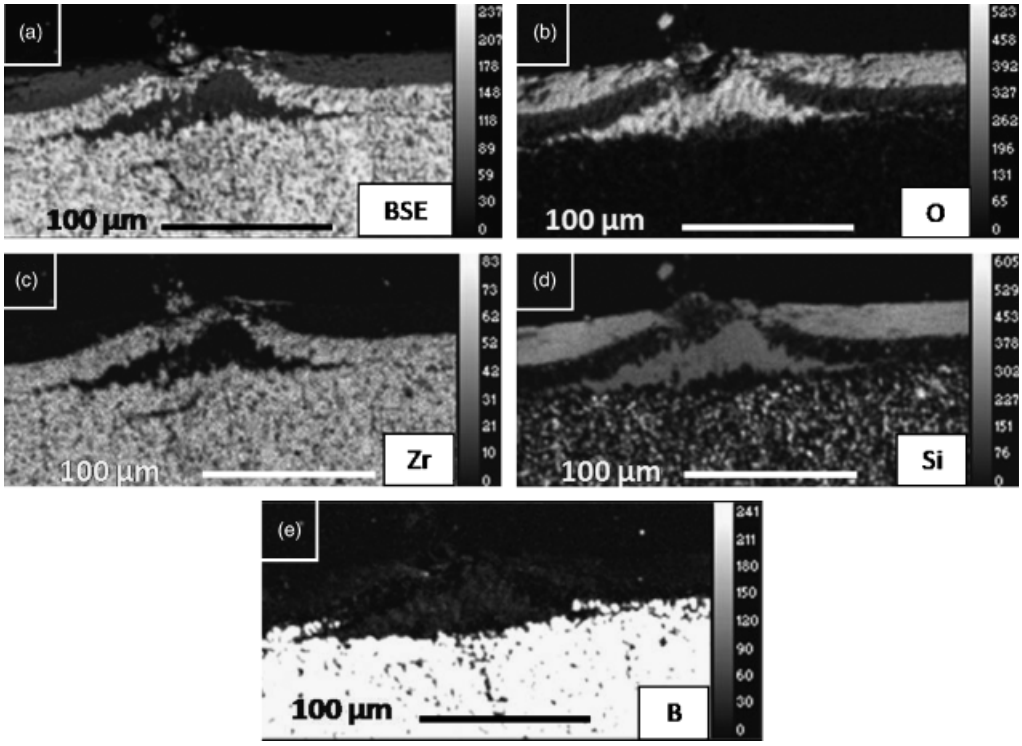

Fig. 5. (a) Backscattered electron (BSE) image of a deformation with glass inside located in the cross section of the ZrB_2–15%SiC composite oxidized at 1550°C for 3 h; (b)–(e) the same area as in (a) imaged by electron microprobe analysis in oxygen Ka X-rays (b), zirconium La X-rays (c), silicon Ka X-rays (d), and boron Ka X-rays (e). The scale bars on the elemental maps represent the intensity of the corresponding element. The elemental maps (b)–(e) indicate SiO_2-rich surface layer and underlying ZrO_2 layer as well as the composition of the BSZ glass inside the deformation.

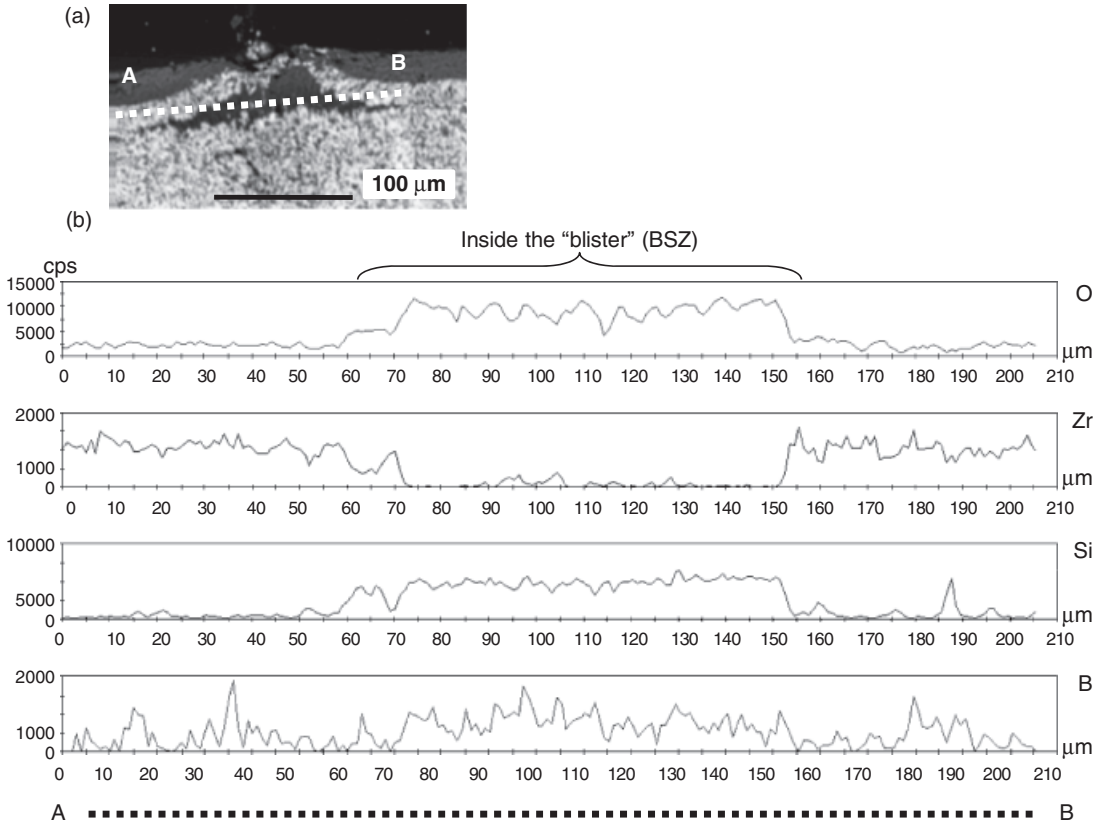

Fig. 6. (a) Backscattered electron image of a cross section of a cell on surface of a ZrB_2–15 vol% SiC composite oxidized at 1550°C for 3 h. The white line through the "blister" (deformation) indicates where the EPMA line analyses were done; the letter A indicates the start of the line scan and B the end (b) graphs of the recorded intensity ((Cps) counts per second) versus distance (µm) of the line scan.

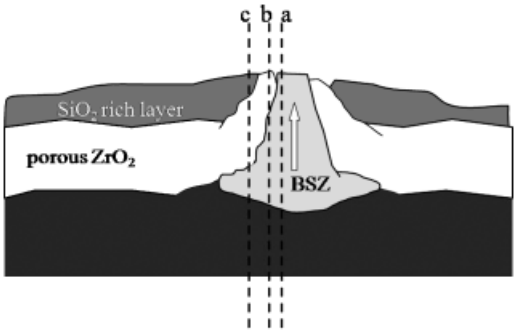

Fig. 7. Schematic showing different planes of cross sections possible through a convection cell, showing the inner structure of the cell.

the ZrO_2 "island", suggesting this to be the glass of the B_2O_3-rich BSZ liquid. Note that the interface between the "primary" ZrO_2 subscale and the unoxidized ZrB_2–SiC substrate extends about 100 μm beneath the surface under the ZrO_2 "island" (the center of the convection cell) but only about 50 μm away from the center of the convection cell. Apparently this increased subscale recession of the ZrB_2–SiC substrate denotes faster oxidation at this location.

When interpreting the cross-sectional images of the deformations shown in Fig. 4, one needs to consider that because the location of the plane of polish is not known, it is hard to infer if the features seen differ because of their location, or if they differ because they have not developed (immature or "before eruption") or have stopped operating ("extinct"). Figure 7 is an illustration of a convection cell intersected by several planes of cross section for polish. Line "a" in Fig. 7 intersects the center of a BSZ liquid pipe. This can create an image similar to Fig. 4(d). If the plane of polish intersects the side of a convection cell (through a ZrO_2 "island" filled with liquid), i.e. line "b", it could create an image similar to Fig. 4(c), while a plane of polish more remote from the pipe (line "c") could create an image similar to Fig. 4(b).

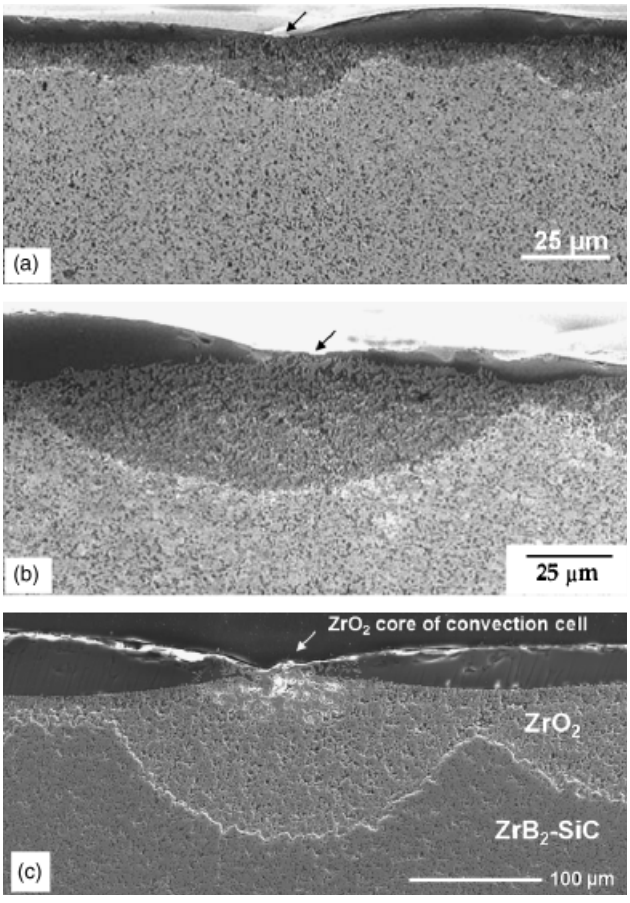

Fig. 8. Scanning electron microscopic images of the cross sections of diboride/silicon carbide composites. (a) HfB_2–SiC–HfN and (b) ZrB_2–HfB_2–SiC–HfN composites oxidized at 1450°C for 20 h by Monteverde[12]; (c) a ZrB_2–15%SiC composite oxidized at 1550°C for 2 h.

IV. Comparison with Literature

Microstructural features closely resembling the convection cells have been reported earlier in the literature but not interpreted as of significance. Figure 8 compares previously published images of specimens oxidized at CNR-ISTEC by Monteverde[12] with a specimen oxidized at University of Michigan (UM). Cross sections of HfB_2–SiC–HfN and ZrB_2–HfB_2–SiC–HfN composites oxidized at 1450°C for 20 h by Monteverde[12] at CNR-ISTE are shown in Figs. 8(a) and (b). The images show vertical ZrO_2 features on top of an enhanced oxidation zone (increased thickness of ZrO_2 layer). Figure 8(c) shows a ZrB_2–15 vol% SiC composite fabricated at CNR-ISTEC and oxidized at 1550°C for 2 h at UM. The cross sections shown in Figs. 8(a) and (b) closely resemble the cross section of the convection cell shown in Fig. 8(c). Note the similarity in the morphology of the vertical ZrO_2 feature of the specimens oxidized at CNR-ISTEC to the morphology of the ZrO_2 "island" of the specimen oxidized at UM (indicated by a arrow in Fig. 8). Also, all three specimens shown in Fig. 8 have thicker ZrO_2 layer (enhanced oxidation zone) under the vertical ZrO_2 features. The similarity of these images indicate that the convection cells are seen in other boride–SiC materials such as these Hf(Zr)B_2–SiC–HfN composites, which have a different relative amount of in Hf(Zr)O_2, SiO_2, and B_2O_3 after oxidation.

Figure 9(a) shows similar features for a ZrB_2–30 vol% SiC composite oxidized for 30 min at 1400°C by Rezaie *et al.*[13] at the University of Missouri-Rolla (UMR) previously reported in the literature. Figure 9(b) shows a cross section of a ZrB_2–15 vol% SiC composite (fabricated at CNR-ISTEC) oxidized for 1 h at 1550°C at UM. The cross sections have very similar microstructural features: enhanced oxidation zone (thicker ZrO_2 layer) under a vertical ZrO_2 feature. This indicates that convection cells were formed on the ZrB_2–30 vol% SiC composite during

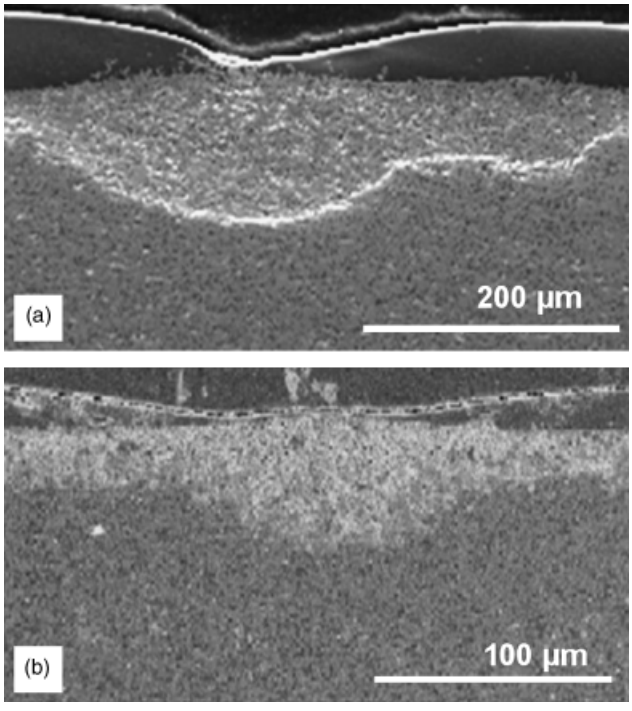

Fig. 9. Cross sections of ZrB_2–SiC composites. (a) ZrB_2–15%SiC oxidized at 1550°C for 1 h and (b) ZrB_2–30 vol% SiC oxidized at 1400°C for 30 min by Rezaie *et al.*[13]

oxidation. Figure 10(a) shows a micrograph of the surface of the ZrB_2–SiC specimen oxidized for 1 h at 1550°C at UM. The image shows how the convection cells are spread over the surface, forming a pattern with small micrometer-sized ZrO_2 particles located between the boundaries of the cells. Figure 10(b) shows the flow pattern of the ZrO_2 particles in more detail. No micrographs of the surfaces of the specimens oxidized at CNR-ISTEC or UMR were reported; thus comparison of these surfaces to the UM specimens could not be done.

The features shown in previously published micrographs from CNR-ISTEC and UMR are suggested here to be in fact convection cells. These findings indicate that the convection cells do exist for other oxidized boride–SiC materials but have not been brought to attention in the literature or interpreted as of significance for the oxidation behavior of these materials.

V. Subscale Recession: Enhanced Oxidation Regions

Now let us direct our attention to the local regions of enhances oxidation shown in Figs. 4(d), 8 and 9. These are the areas with more diboride recession (deeper) and thicker oxide scales (thicker ZrO_2 layer) under the convection cell features. Why do these form? Our hypothesis is based on inward diffusion of oxygen. Let us assume that the rate of diboride oxidation is limited by inward oxygen transport as has been reported previously in the UHTC literature.[2,13,14] Areas of greater recession demand greater inward oxygen diffusion to leave a thicker scale. The driving force is similar; hence, the oxygen diffusivity must be locally higher. Here we can invoke the Stokes–Einstein relation[15] between diffusivity and viscosity, derived from studies of the Brownian motion of a solid sphere suspended in a fluid, where the particle's diffusivity is inversely proportional to the fluid viscosity, i.e. $D \sim 1/\eta$, more specifically[15–17]

$$D = \frac{k_B T}{6\pi\eta r} \tag{1}$$

where D is the diffusion coefficient, k_B the Boltzmann constant, r is the radius of the slowest particle moving through the fluid (the hydrodynamic radius), and T the absolute temperature. Another similar equation based on the theory of absolute reaction rates by Eyring[18] is sometimes preferred for silicate glasses to relate melt viscosities to the diffusion coefficients of oxygen in molten silicates[16,18,19]:

$$D = \frac{k_B T}{\lambda\eta} \tag{2}$$

where λ is the mean jump distance of the diffusing particle (O^{-2}).

In the SiO_2-rich scale, the viscosity at oxidation temperatures of 1500°C is on the order of 10^{11} Poise (10^{10} Pa · s).[20] With the presumed composition of BSZ liquid,[10] we have estimated based on limited data in the literature that the viscosity will be about 10^4 Poise (10^3 Pa · s)[8,9,20]; this is a large viscosity difference, by about factor of 10^7. This implies that in the local regions of the BSZ liquid pipes, the diffusivity for inward diffusion of oxygen must be larger by a similar factor, about 10^7 times faster oxygen transport than in the SiO_2 scale remote from the pipe. When the convection cell forms (the deformation erupts) outward flow of material of low viscosity (BSZ liquid) occurs and a localized inward path for oxygen will be created. A synergy between oxygen transport in and liquid transport out occurs. Thus we expect a complex coupling of these phenomena.

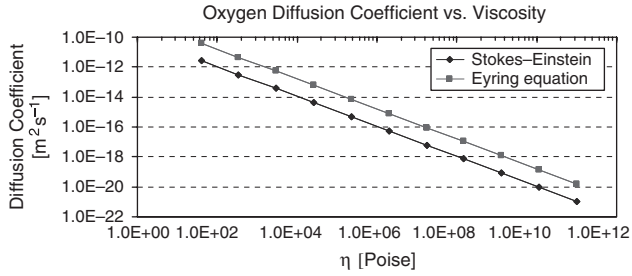

Fig. 11. Diffusion coefficient of oxygen in a B_2O_3–SiO_2 melt at 1550°C calculated by using the Stokes–Einstein relation (diamonds) and the Eyring equation (squares) versus the shear viscosity (logarithmic scale).

Oxygen can diffuse through amorphous SiO_2 via two mechanisms: (1) so-called network oxygen ions can diffuse through the SiO_4 tetrahedral network and (2) interstitial (nominally molecular) oxygen can diffuse through the free volume of the silicate structure.[21] For the network oxygen ion diffusion the Eyring can be used to estimate the oxygen diffusion coefficient by using λ as the mean jump distance of the diffusing particle (O^{-2}).[16,18,19] The diffusion coefficient of interstitial oxygen diffusion (molecular) can be estimated by using the Stokes–Einstein relation with r (hydrodynamic radius) substituted by the O_2 bond length (1.21 Å).[22] The two mechanisms can operate simultaneously and most likely have different temperature dependencies. Thus oxidation at different temperatures could be governed by either mechanism.[21] The question of whether oxygen diffuses through SiO_2 as a molecule or ionically or perhaps both remains unclear, which has led to a broad range of reported diffusion coefficients.[16,17,19,21–28]

Figure 11 shows the calculated diffusion coefficient of oxygen in a borosilicate melt versus the viscosity, calculated with the Stokes–Einstein relation and the Eyring equation. For the Stokes–Einstein relation the following parameter were used; $T = 1550$°C, and $r = 1.21$ nm (where the O_2 bond length is used for the hydrodynamic radius of O_2[22]) and viscosity values are estimated by relationship extrapolated from data by Jabra and colleagues.[9,20] The same viscosity values were used for the Eyring equation as well as $T = 1550$°C, and $\lambda = 0.159$ nm, which is the Si–O distance in SiO_2 glass.[19] The diffusion coefficients

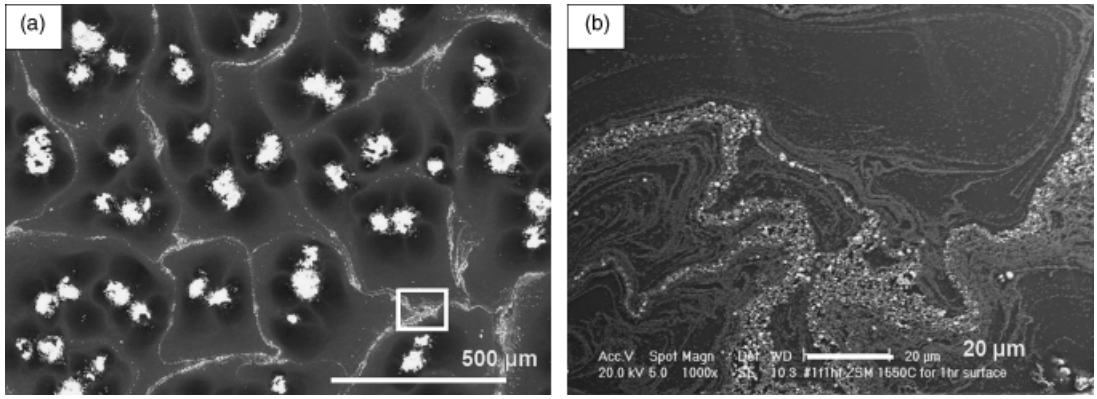

Fig. 10. Backscattered electron images of the surface of a ZrB_2–SiC composite oxidized at 1550°C for 1 h shown earlier in cross-sectional view in Fig. 10(b); (a) low magnification (b) high magnification of the area inside the white box in (a).

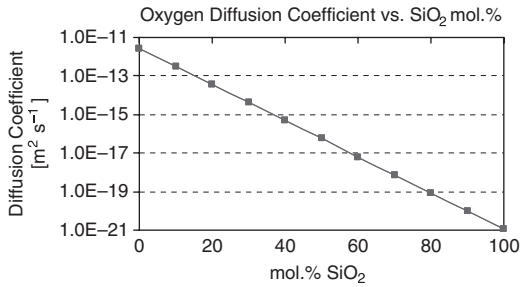

Fig. 12. Diffusion coefficient of oxygen in a B_2O_3–SiO_2 melt versus SiO_2 mol% calculated using the Stokes–Einstein relation.

calculated by the two equations differ on the order of about one magnitude. The difference is not large compared with the wide range of values reported in the literature; also these values are comparable to measured and calculated values reported previously.[16,17,19,21–29]

Figure 12 shows the diffusion coefficient of oxygen in a borosilicate melt versus mol% of SiO_2 estimated by using the Stokes–Einstein relation with $T = 1550°C$, $r = 0.121$ nm, and viscosity values estimated from data by Jabra and colleagues.[9,20] Figure 12 shows how the inward oxygen diffusion decreases with an increase in SiO_2 mol% in a B_2O_3–SiO_2 melt. This is indicated by the low diffusion coefficient of oxygen for a pure SiO_2 melt (100 mol% SiO_2; $D = 1.1 \times 10^{-21}$ m^2/s) compared with a B_2O_3-rich melt (79 mol% B_2O_3–21 mol% SiO_2; $D = 1.7 \times 10^{-14}$ m^2/s), which is 10^7 times larger, as estimated from the large viscosity difference mentioned above. The calculated diffusion coefficients of oxygen in borosilicate melts (Fig. 12) is smaller than the diffusion coefficient for oxygen in ZrO_2 ($\sim 10^{-10}$ m^2/s at 1500°C) reported by Fox and Clyne[28] supporting our previous assumption that the borosilicate outer layer is the oxygen diffusion barrier (the rate controlling factor) during oxidation at these temperatures.

The local enhanced oxidation regions under the convection cells makes the oxidation of diboride–SiC composites at these temperatures a nonuniform process at a microscopic scale. Observations of apparently uniform oxidation behavior reported in the literature could result from the fine scale of the local events. Just like an intergranular corrosion may be quite homogenous on the macroscopic scale, it is though localized on a microscopic scale.[30] Perhaps in the early state of the oxidation uniform oxygen diffusion generates a pool of BSZ liquid. When the volume of the liquid and the pressure (by Pillings–Bedworth ratio) reaches a critical amount, it erupts. While it is erupting, oxygen can diffuse in by the same path; hence, it oxidizes faster under a cell creating the enhanced oxidation zone.

VI. Summary

Oxide scale features previously published in the literature on ZrB_2–SiC and HfB_2–SiC composites are suggested here to be in fact the proposed convection cells reported for the first time by the authors.[9] These features are of great significance contributing to the formation of complex oxide scales of these materials. The flow of a B_2O_3-rich BSZ liquid to the surface, with the subsequent loss of B_2O_3 to evaporation, explains the formation of a glassy SiO_2-rich layer on the surface commonly reported in the literature. Also the outward flow of the BSZ liquid creates a localized inward path for oxygen due to lower viscosity that allows faster oxidation under the convection cell. The formation of a convection cell (eruption of the "primary" scale) creates a leak in the SiO_2 barrier, but the BSZ liquid eventually replenishes the SiO_2 scale, patching the leak creating a positive feedback.

Acknowledgments

We thank Dr. David Shifler of the Office of Naval Research for supporting the research under contract N00014-02-1-0034 and Drs. Alida Bellosi, Frederick Monteverde, Gregory Hilmas, and William Farhenholtz for providing samples and valuable discussions.

References

[1]F. Monteverde and A. Bellosi, "The Resistance to Oxidation of HfB_2–SiC Composite," *J. Eur. Ceram. Soc.*, **25**, 1025–31 (2005).
[2]F. Monteverde and A. Bellosi, "Oxidation of ZrB_2-Based Ceramics in Dry Air," *J. Electrochem. Soc.*, **150** [11] B552–9 (2003).
[3]A. Chamberlain, W. Fahrenholtz, G. Hilmas, and D. Ellerby, "Oxidation of ZrB_2–SiC Ceramics Under Atmospheric and Reentry Conditions," *Refract. Appl. Trans.*, **1** [2] 1–8 (2005).
[4]S. R. Levine, E. J. Opila, M. C. Halbig, J. D. Kiser, M. Singh, and J. A. Salem, "Evaluation of Ultra-High Temperature Ceramics for Aeropropulsion Use," *J. Eur. Ceram. Soc.*, **22**, 2757–67 (2002).
[5]W. G. Fahrenholtz, "Thermodynamic Analysis of ZrB_2–SiC Oxidation: Formation of a SiC-Depleted Region," *J. Am. Ceram. Soc.*, **90** [1] 143–8 (2007).
[6]M. M. Opeka, I. G. Talmy, and J. A. Zaykoski, "Oxidation-Based Materials Selection for 2000°C+Hypersonic Aerosurface: Theoretical Considerations and Historical Experience," *J. Mater. Sci.*, **39** [19] 5887–904 (2004).
[7]A. Bongiorno, C. J. Först, R. K. Kalia, J. Li, J. Marschall, A. Nakano, M. M. Opeka, I. G. Talmy, P. Vashishta, and S. Yip, "A Perspective on Modeling Material in Extreme Environments: Oxidation of Ultra-High Temperature Ceramics," *Mater. Res. Soc. Bull.*, **31**, 410–8 (2006).
[8]P. C. Setze, *A Review of the Physical and Thermodynamic Properties of Boric Oxide. NACA-RM-E57B14*. Lewis Flight Propulsion Laboratory, Cleveland, OH, 1957.
[9]S. N. Karlsdottir, J. W. Halloran, and C. E. Henderson, "Convection Patterns in Liquid Oxide Films on Zirconium Diboride–Silicon Carbide Composites Oxidized at High Temperature," *J. Am. Ceram. Soc.*, **90** [9] 2863–7 (2007).
[10]S. N. Karlsdottir, J. W. Halloran, and A. N. Grundy, "Zirconia Transport by Liquid Convection During Oxidation of Zirconium Diboride–Silicon Carbide Composite," *J. Am. Ceram. Soc.*, **91** [1] 272–7 (2008).
[11]S. N. Karlsdottir, J. W. Halloran, F. Monteverde, and A. Bellosi, "Oxidation of ZrB2-SiC: Comparison of Furnace Heated Coupons and Self-Heated Ribbon Specimens"; in *Proceedings of the 31st International Conference on Ceramics and Composites, Daytona Beach FL, January 21–26, 2007. Mechanical Properties and Performance of Engineering Ceramics and Composites III*, Edited by E. Lara-Curzio. *Ceram. Trans.*, **28** [2] 327–336 (2007).
[12]F. Monteverde, "The Thermal Stability in Air of Hot Pressed Diboride Matrix Composites for Uses at Ultra-High Temperatures," *Corros. Sci.*, **47**, 2020–33 (2005).
[13]A. Rezaie, W. G. Fahrenholtz, and G. E. Hilmas, "Evolution of Structure During the Oxidation of Zirconium Diboride–Silicon Carbide in Air up to 1500°C," *J. Eur. Ceram. Soc.*, **27** [6] 2495–501 (2007).
[14]F. Monteverde, "Beneficial Effects of an Ultra-Fine α-SiC Incorporation on the Sinterability and Mechanical Properties of ZrB_2," *Appl. Phys. A*, **82**, 329–37 (2006).
[15]A. Einstein, *Investigations on the Theory of the Brownian Movement*, reprinted by Dover Publications, New York, 1926.
[16]Y. Liang, F. M. Richter, A. M. Davis, and E. B. Watson, "Diffusion in Silicate Melts: I. Self Diffusion in CaO–Al_2O_3–SiO_2 at 1500°C and 1 GPa," *Geochim. Cosmochim. Acta*, **60** [22] 4353–67 (1996).
[17]E. M. Tanguep Njiokep and H. Mehrer, "Diffusion of ^{22}Na and ^{45}Ca in Ionic Conduction in Two Standard Soda-Lime Glasses," *Solid State Ionics*, **177**, 2839–44 (2006).
[18]H. Eyring, "Viscosity, Plasticity, and Diffusion as Examples of Absolute Reaction Rates," *J. Chem. Phys.*, **4** [4] 283–91 (1936).
[19]M. L. Ferreira Nascimento and E. D. Zanotto, "Mechanisms and Dynamics of Crystal Growth, Viscous Flow, and Self-Diffusion in Silica Glass," *Phys. Rev. B*, **73**, 024209 (2006).
[20]R. Jabra, J. Phalippau, and J. Zarzicki, "Synthesis of Binary Glass-Forming Oxide Glasses by Hot-Pressing," *J. Non-Cryst. Solids*, **42**, 489–98 (1980).
[21]C. E. Ramberg and W. L. Worrell, "Oxygen Transport in Silica at High Temperatures: Implications of Oxidation Kinetics," *J. Am. Ceram. Soc.*, **84** [11] 2607–16 (2001).
[22]J. Read, K. Mutolo, M. Ervin, W. Behl, J. Wolfenstine, A. Driedger, and D. Foster, "Oxygen Transport Properties of Organic Electrolytes and Performance of Lithium/Oxygen Battery," *J. Electrochem. Soc.*, **150** [10] A1351–6 (2003).
[23]R. H. Doremus, "Transport of Oxygen in Silicate Glasses," *J. Non-Cryst. Solids*, **349**, 242–7 (2004).
[24]Y. Zhang, E. M. Stolper, and G. J. Wasserburg, "Diffusion of a Multi-Species Component and its Role in Oxygen and Water Transport in Silicates," *Earth Planet Sci. Lett.*, **103**, 228–40 (1991).
[25]E. L. Williams, "Diffusion of Oxygen in Fused Silica," *J. Am. Ceram. Soc.*, **48** [4] 190–4 (1965).
[26]D. Tinker, C. E. Lesher, and I. D. Hutcheon, "Self-Diffusion of Si and O in Diopside Anorthite Melt at High Pressure," *Geochim. Cosmochim. Acta*, **67** [1] 133–42 (2003).
[27]F. J. Norton, "Permeation of Gaseous Oxygen Through Vitreous Silica," *Nature*, **191**, 701 (1961).
[28]A. C. Fox and T. W. Clyne, "Oxygen Transport by Gas Permeation Through the Zirconia layer in Plasma Sprayed Thermal Barrier Coatings," *Surf. Coat. Technol.*, **184**, 311–21 (2004).
[29]J. D. Cawley, J. W. Halloran, and A. R. Cooper, "Oxygen-18 Tracer Study of the Passive Thermal Oxidation of Silicon," *Oxid. Met.*, **28** [1–2] 1–15 (1987).
[30]R. Telle, L. S. Sigl, and K. Takagi, "Transition Metal Boride Ceramics"; pp. 140–54 in *Handbook of Ceramic Hard Materials*, Vol. 1, Edited by R. Reidel. Wiley-VCH, Weinheim, Germany, 2000. □